bioRxiv preprint doi: https://doi.org/10.1101/206888; this version posted October 27, 2017. The copyright holder for this preprint (which was not certified by peer review) is the author/funder. All rights reserved. No reuse allowed without permission.

In vivo cross-linking and transmembrane helix dynamics support a non-piston model of signalling within *E. coli* EnvZ

Rahmi Yusuf[a,1], Tuyết Linh Nguyễn[a,1], Annika Heininger[b], Robert J. Lawrence[a], Benjamin A. Hall[c*] and Roger R. Draheim[a,d*]

[a]School of Pharmacy and Biomedical Sciences, University of Portsmouth, Portsmouth, PO1 2DT, England, UK; [b]Institute of Biochemistry, Biocenter, Goethe University Frankfurt, D-60438 Frankfurt, Germany; [c]MRC Cancer Unit, University of Cambridge, Cambridge, CB2 0XZ, England, UK; [d]Institute of Biological and Biomedical Science, University of Portsmouth, Portsmouth, PO1 2DT, England, UK

Running title: Non-piston transmembrane communication by EnvZ

[1]These authors contributed equally

*To whom correspondence should be addressed (B. A. H. or R. R. D.):

MRC Cancer Unit
University of Cambridge
Hutchison / MRC Research Centre
Box 197, Cambridge Medical Campus
Cambridge
CB2 0XZ
United Kingdom
tel: + 44 (0) 1223 763240
fax: + 44 (0) 1223 763241

University of Portsmouth
School of Pharmacy and Biomedical Sciences
St. Michael's Building
White Swan Road
Portsmouth
PO1 2DT
United Kingdom
tel: +44 (0)23 9284 2133
fax: +44 (0)23 9284 3565

bioRxiv preprint doi: https://doi.org/10.1101/206888; this version posted October 27, 2017. The copyright holder for this preprint (which was not certified by peer review) is the author/funder. All rights reserved. No reuse allowed without permission.

Keywords

porin balance / transmembrane communication / coarse-grained molecular dynamics / sulfhydryl-reactivity / transmembrane helix dynamics

bioRxiv preprint doi: https://doi.org/10.1101/206888; this version posted October 27, 2017. The copyright holder for this preprint (which was not certified by peer review) is the author/funder. All rights reserved. No reuse allowed without permission.

In gram-negative bacteria, porins span the outer membrane and control the influx of several prominent groups of antibiotics[1,2]. Thus, it should not be surprising that expression of these porins is often altered in clinical isolates that exhibit multidrug resistance (MDR)[3-9]. The major regulator of porin expression in *Escherichia coli* is EnvZ, a canonical sensor histidine kinase (SHK). It allosterically processes periplasmic interactions with MzrA and cytoplasmic osmosensing into a single unified change in the ratio of its kinase and phosphatase activities[10-15]. Unfortunately, the role of the transmembrane domain (TMD) in communicating these signals across the cellular membrane remains not well understood. Here, we employed *in vivo* sulfhydryl-reactivity to probe the dynamics of individual TM2 helices within the TMD and demonstrate that upon stimulus perception, EnvZ employs a non-piston-type mechanism of transmembrane communication. *In silico* coarse-grained molecular dynamics (CG-MD) simulations with EnvZ TM2 are in agreement with these *in vivo* results. We conclude by discussing these results within the context of allosteric processing by EnvZ and propose that these results can be used to predict and classify transmembrane communication by various SHKs.

Most porins involved in antibiotic transport by gram-negative bacteria belong to the classical OmpF and OmpC families[2]. Transcription of these porins is governed by the intracellular concentration of phospho-OmpR (OmpR-P), which is controlled by EnvZ in response to changes in periplasmic interactions with MzrA and environmental osmolarity[10-15] (Figure S1A). At low intracellular levels of OmpR-P, transcription of *ompF* is upregulated, whereas at higher levels of OmpR-P, transcription of *ompF* is repressed and transcription of *ompC* is activated. This results in a predominance of OmpF at low osmolarity and OmpC at higher osmolarities or in the presence of MzrA (Figure S1B)[16-18]. Dramatic modification of porin balance, which has been observed within clinical isolates from patients undergoing antibiotic treatment, strongly suggests that the underlying mechanisms of porin regulation by EnvZ require further characterisation[3-9]. In addition, it was

bioRxiv preprint doi: https://doi.org/10.1101/206888; this version posted October 27, 2017. The copyright holder for this preprint (which was not certified by peer review) is the author/funder. All rights reserved. No reuse allowed without permission.

recently shown that mutations in EnvZ within a porin-deficient (*ompC*⁻ *ompF*⁻) *E. coli* strain also resulted in increased carbapenem resistance[19]. Thus, EnvZ plays a not well-understood role in mediating antibacterial resistance that warrants further elucidation.

Comparison of recently published *apo* and *holo* high-resolution (~1.9 Å) crystal structures of the *E. coli* nitrate sensor NarQ that contain the periplasmic, TM and HAMP domains reveal extensive structural rearrangements involving a piston-like motion of TM1 relative to TM2 of approximately 2.5 Å. These displacements result in a lever-like rotation of individual HAMP domains upon binding of cognate ligand[20]. Based on these results, the authors posit that receptors containing a membrane-adjacent HAMP domain function by a piston-type displacement of TM helices while those that lack such domains transduce signal by rotation of TM helices. We previously postulated a related yet different categorisation of signalling mechanisms also based on the domain structure of bacterial receptors[21]. We proposed that receptors containing a periplasmic four-helix bundle transduce signal across the membrane by piston-type displacements and that the attached membrane-adjacent HAMP domains might possess one of a multitude of signalling mechanisms including a gearbox-type rotation[22], a dynamic bundle[23] or potentially other mechanisms[21]. Differentiating between these classification systems will provide a theoretical framework for understanding domain-based intra-protein allosteric communication by bacterial receptors.

Here, we have analysed transmembrane signalling within EnvZ for several reasons. Firstly, because of its aforementioned importance in regulating bacterial porin expression. Understanding how EnvZ transduces signal would be a significant step toward direct manipulation of porin balance in bacterial cells exhibiting MDR. Secondly, it examines whether SHKs that possess membrane-adjacent HAMP domains function solely by piston-type displacements or whether other signalling mechanisms might be employed. The results here with EnvZ are compared with previous findings

bioRxiv preprint doi: https://doi.org/10.1101/206888; this version posted October 27, 2017. The copyright holder for this preprint (which was not certified by peer review) is the author/funder. All rights reserved. No reuse allowed without permission.

from the aspartate chemoreceptor (Tar) and the recent NarQ structures[20,24-26]. These three are ideal candidates for comparison because they all possess a membrane-adjacent HAMP domain, however, while Tar and NarQ possess a periplasmic four-helix bundle, EnvZ possesses a periplasmic PDC/CACHE domain[27,28].

Mapping TM2 surfaces important for EnvZ signal output

We previously created a Cys-less version of EnvZ from *E. coli* that had its sole Cys residue changed to an Ala residue (C277A). The Cys-less variant is expressed from pRD400, which results in the addition of a seven-residue linker (GGSSAAG) and a C-terminal V5 epitope (GKPIPNPLLGLDST). We previously found that the Cys-less version of EnvZ had similar steady-state signal output and response to environmental osmolarity as the wild-type version of EnvZ making it suitable for comparisons of *in vivo* sulfhydryl-reactivity and signal output analysis. We initially determined that no major rearrangements occur along the TM1-TM1' interface upon stimulus perception[29]. As minimal change was observed along this helical interface in response to osmolarity, we continued by examining the TM2-TM2' interface. We began by determining which residues comprise TM2 by subjecting the full EnvZ sequence to DGpred[30] and TMHMM v2.0[31], which suggested that Leu-160 to Ile-181 and Leu-160 to Ile-179 comprise TM2 respectively. Based on these analyses, we employed site-directed mutagenesis using the Cys-less variant as a template to create a library of single-Cys-containing EnvZ proteins that spanned from positions 156 to 184 (Figure 1). We observed that nearly the entire library was expressed within EPB30/pRD400 cells grown under the low- or high-osmolarity regime. Variants possessing a Cys at position 156 showed low levels of expression when grown under the low-osmolarity (0% sucrose) regime. However, when grown under the high-osmolarity regime, no variants showed reduced expression level (Figure S2). These results indicate that the library is suitable for further *in vivo* experimentation.

bioRxiv preprint doi: https://doi.org/10.1101/206888; this version posted October 27, 2017. The copyright holder for this preprint (which was not certified by peer review) is the author/funder. All rights reserved. No reuse allowed without permission.

We began by expressing each of the single-Cys-containing variants in EPB30/pRD400 cells, which allowed us to measure CFP fluorescence, YFP fluorescence, and to calculate the CFP/YFP ratio that estimates steady-state EnvZ signal output (Figure S1B). Cells expressing the Cys-less C277A were used as a baseline comparison (Figure S3). When EPB30/pRD400 cells are grown under the low-osmolarity regime, a shift in signalling output toward the "on" or kinase-dominant state results in increased CFP fluorescence, reduced YFP fluorescence and an increase in the overall CFP/YFP ratio, while a shift toward the "off" or phosphatase-dominant state appears as decreased CFP, increased YFP and a decrease in CFP/YFP ratio (Figures 2 and S4).

Several trends were observed during analysis of the library of Cys-containing EnvZ receptors. When EPB30/pRD400 cells were grown under the low-osmolarity regime, EnvZ was less tolerant of Cys substitutions at the N- and C-terminal regions of the library. At the N-terminus, signal output from receptors containing a Cys at positions 156, 162 and 163 were very elevated, exhibiting greater than a 5-fold increase in CFP/YFP, while receptors possessing a Cys in the C-terminus at positions 179, 181, 182 and 184 were elevated, possessing over a 2-fold increase in CFP/YFP. These boundary regions appear to flank a core of alternating increases and decreases in EnvZ signal output, as observed between residue positions 165 and 180, suggesting that multiple tightly packed EnvZ helices exist within the hydrophobic core of the inner membrane (Figures 2A and 2B). When grown under the high-osmolarity regime, a pattern appeared where Cys substitutions resulted in significant decreases in signal output (Figure 2C). Of the 29 mutants analysed, 13 supported less than 75% of the normal wild-type signal output.

Perhaps most striking is the inverse effect on EnvZ signal output of the Cys substitutions that flank the hydrophobic core of TM2. For these residues, when grown under the low-osmolarity regime, the

bioRxiv preprint doi: https://doi.org/10.1101/206888; this version posted October 27, 2017. The copyright holder for this preprint (which was not certified by peer review) is the author/funder. All rights reserved. No reuse allowed without permission.

presence of a Cys residue resulted in an increase in signal output of more than 25%, i.e. shifted toward the on or kinase-dominant state (red dots in Figure 2A) and a reduction in signal output of more than 25%, i.e. shifted toward the off or phosphate-dominant state, when grown under the high-osmolarity regime (blue dots in Figure 2C). These flipped positions reside at the N- and C-terminal ends of the region we examined and outside of the proposed hydrophobic TMD core (Figure 2). Within the hydrophobic core, Cys substitutions show similar changes when cells are grown under the low- and high-osmolality regimes. These results suggest that the flanking regions are not simply rigid structural conduits for signal transduction but may have higher-order roles in signal transduction, such as MzrA interaction or functioning as a control cable at the N- and C-terminal regions respectively[14,15,23,32-34].

Identifying surfaces involved in TM2-TM2' interactions

Sulfhydryl-reactivity experimentation is well-characterised and has been employed on many soluble and membrane-spanning proteins and higher-order complexes[35]. The *in vivo* nature of this assay facilitated mapping of the TM2-TM2' interface under different osmotic conditions, which is an important first step toward understanding how EnvZ processes allosteric inputs from periplasmic MzrA binding and cytoplasmic osmosensing into a single uniform modulation of bacterial porin balance (Figures 1 and S1). In a similar manner to mapping TM1-TM1' interactions[29], Cys-containing EnvZ variants were expressed in EPB30/pRD400 cells and upon entering the early exponential phase ($OD_{600nm} \approx 0.25$) they were subjected to 250 μM molecular iodine for 10 minutes analysed by non-reducing SDS-PAGE and immunoblotting (Figure S5).

We observed three distinct regions within TM2. The N-terminal region (region I in Figure 3), comprised of residues 156 to 163, exhibited significant cross-linking under the low-osmolarity

bioRxiv preprint doi: https://doi.org/10.1101/206888; this version posted October 27, 2017. The copyright holder for this preprint (which was not certified by peer review) is the author/funder. All rights reserved. No reuse allowed without permission.

regime (0% sucrose) and almost no crosslinking under the high-osmolarity (15% sucrose) regime. The second region (II) consisting of positions 164 to 179, demonstrated altering low and high levels of disulphide-formation consistent the crossing of TM2 and TM2' within the hydrophobic core of the TMD. The final region (III), from residues 180 to 184, shows no crosslinking (Figure 3). It should be noted that this significant difference at the periplasmic end of the TMD between cells grown under the low- and high-osmolarity regime was not observed during similar analyses of TM1[29].

Molecular simulations of the wild-type and aromatically tuned variants of EnvZ TM2

The piston-type model of transmembrane communication is founded upon the central tenant that the vertical position of TM2 relative to the lipid bilayer changes upon stimulus perception. Previous work with TM2 of Tar demonstrates that repositioning the aromatic residues at the cytoplasmic end of TM2, known as aromatic tuning[36], repositions the helix within a biological membrane[37] and that this repositioning causes an incremental change in signal output[36]. These results served as an experimental framework to optimise SIDEKICK software capable of high-throughput parallelised coarse-grained molecular dynamics (CG-MD) simulations, which demonstrated that aromatic tuning repositioned the TM2 helix *in silico* in a manner consistent with both the *in vivo* results and a piston-type mechanism of transmembrane communication[38].

Based on these extensive results and the recent suggestion that mechanisms employed by SHKs during TM communication correlate with the presence of a membrane-adjacent HAMP domain, we performed analogous *in silico* experimentation with EnvZ, which possesses a membrane-adjacent HAMP domain but substitutes a periplasmic PDC/CACHE domain for the four-helix bundle present in Tar and NarQ[20,27,28,39]. We previously performed aromatic tuning with TM2 of EnvZ and found

bioRxiv preprint doi: https://doi.org/10.1101/206888; this version posted October 27, 2017. The copyright holder for this preprint (which was not certified by peer review) is the author/funder. All rights reserved. No reuse allowed without permission.

that signal output was not correlated with the absolute vertical position of the aromatic residues as was shown for Tar TM2, which suggested that EnvZ does not transduce signal output across the membrane by a piston-type displacement[40].

To interpret the results of our GC-MD analysis, we categorised the signal output of these aromatically tuned EnvZ variants[40]. For several two-component signalling circuits, including the EnvZ/OmpR, PhoQ/PhoP and CpxA/CpxR circuits, the steady-state output of the signalling circuits has been shown to be independent of the level of SHK present[40-43]. However, in circuits containing the tuned variants of EnvZ, a different relationship between steady-state signal output and receptor level was observed, suggesting that the ratio of kinase to phosphatase activities was different within each receptor and always different than wild-type EnvZ[40]. Based on this analysis, we found that the WLF-1 variant possessed the highest signal output while the WLF-5, WLF-4 and WLF-3 variants possessed only slightly higher activity than wild-type EnvZ, which maintained receptor-concentration dependent robustness unlike the tuned variants. WLF-2 and WLF+1 were found to possess reduced signal output, while WLF+2 possessed the lowest overall signal output. These differences were previously quantified by analysing the slope of the change in CFP/YFP against the amount of receptor present and are visually represented in Figure S6[40]. These classifications are employed during interpretation of the CG-MD results in Figure 4.

Based on these previous results and the absence of asymmetric TM2 displacement observed within the *in vivo* sulfhydryl-reactivity assay (Figure 3), we assessed whether molecular simulations would lend credibility to a non-piston type of transmembrane communication employed by EnvZ. We began by designing tuned TM2 sequences to subject to GC-MD simulations that matched those previously used during the aromatic tuning experimentation (Figure 4A). Unlike analogous experimentation with TM2 of Tar, no trend in helix displacement was observed (Figure 4B, Table

bioRxiv preprint doi: https://doi.org/10.1101/206888; this version posted October 27, 2017. The copyright holder for this preprint (which was not certified by peer review) is the author/funder. All rights reserved. No reuse allowed without permission.

S1). This indicates that the mutations do not in isolation move the helix up and down in the membrane and would appear to rule out a pure piston motion as previously observed in Tar[38].

An alternative mechanism for signal transduction is to induce a tilt in the helix relative to the bilayer normal. This was originally proposed in Tar on the basis of crystallographic analysis of the receptor domain[44], and led to the proposal of a "swinging piston" where both displacement and tilt contributed to signal transduction. In addition, this would be consistent with a scissor-type model of TM communication proposed to be utilised by PhoQ[45,46], which possesses a periplasmic PDC/CACHE domain[47]. In testing the tuned EnvZ TM2 helices, a change in the extent of tilting was observed during the CG-MD simulations (Figure 4C, Table S2). It was found that a reduction in tilt, to a mean tilt of between 22 and 24 degrees, compared to the wild-type TM2 sequence with a tilt of approximately 26 degrees correlated with a decreased signal output (phosphatase-biased, dark blue). Interestingly, an increase in tilt to more than 29 degrees correlated with extremely biased signal output, *i.e.* highly kinase-dominant (WLF-1, pink) and highly phosphatase-dominant (WLF+2, bright blue). Taken together, these results demonstrate that tilt, rather than vertical displacement, does correlate with altered signal output from EnvZ.

Finally, a rotational/gearbox model of TMD-HAMP communication has also been proposed for EnvZ[22,48]. Central to this model is that interconversion between the kinase-dominant and phosphatase-dominant signalling states can be accomplished by rotation of the individual HAMP helices in unison by 26 degrees. Within our simulations, we observed some consistency with the gearbox model of HAMP signalling, especially when the WLF-1 helix possessed a mean azimuthal rotation that is 25 degrees different than wild-type EnvZ (pink in Figure 4D). The full-length WLF-1 receptor was determined to the most highly kinase-biased tuned receptor we studied. The TM helix from the most phosphatase-biased receptor (WLF+2) possessed a mean azimuthal rotation of

bioRxiv preprint doi: https://doi.org/10.1101/206888; this version posted October 27, 2017. The copyright holder for this preprint (which was not certified by peer review) is the author/funder. All rights reserved. No reuse allowed without permission.

an additional 15 degrees. For the simulations involving other helices, it was not possible to differentiate them into separate classes.

Here, our *in vivo* analysis demonstrated that only the periplasmic end of EnvZ TM2 undergoes a conformational transition upon stimulus perception suggesting that the asymmetric piston-type displacement employed by Tar is not used by EnvZ. Previously, a linear correlation was observed between the position of the aromatic residue in Tar TM2, the position of the helices *in vitro* and *in silico* and the signal output from each Tar receptor[36,37,40,49]. Here, *in silico* analysis of EnvZ TM2 demonstrates that such a linear correlation is absent suggesting that EnvZ functions by a non-piston mechanism in which both tilting and azimuthal rotation play a substantial role in modulation of signal output (Figure 4).

Correlations between domain composition and mechanisms of signal transduction

The authors of the recent NarQ structures posit that the presence or absence of the membrane-adjacent HAMP domain may be the difference between receptors employing piston-type mechanisms of transmembrane communication as compared to other signalling mechanisms[20]. However, differences employed during transmembrane communication by the Tar and EnvZ TMDs observed here and previously strongly suggest that Tar and EnvZ possess different mechanisms of TM communication. Our previous work analysed AS1 helices from *E. coli* NarX, *E. coli* Tar, *E. coli* EnvZ and Af1503, the HAMP domain resulting in the initial high-resolution structure[22], and found that the Tar and NarX AS1 helices possess similar properties, which AS1 helices from both EnvZ and Af1503 lack. Recent comparisons of the *apo* and ligand-bound structures of the combined periplasmic-TM-HAMP domain from *E. coli* NarQ demonstrate that binding of ligand results in symmetrical displacements of TM1 relative to TM2 of approximately 2.5 Å.[20] These

bioRxiv preprint doi: https://doi.org/10.1101/206888; this version posted October 27, 2017. The copyright holder for this preprint (which was not certified by peer review) is the author/funder. All rights reserved. No reuse allowed without permission.

results are similar to Tar, which functions by asymmetrical TM2 displacement also possesses a periplasmic four-helix-bundle[24-26,39]. Thus, we conclude that *E. coli* EnvZ functions by a non-piston mechanism of transmembrane communication that is different than Tar, NarX and NarQ, which communicate across the membrane by piston-type displacements. Furthermore, we propose that the TM signalling mechanisms can be predicted and assigned based upon the domain(s) present in the periplasmic region of a bacterial TM-spanning receptor.

Methods

Bacterial strains and plasmids

E. coli strains DH10B (New England Biolabs) or MC1061[50] were used for DNA manipulations, while strain K-12 MG1655[51] served a non-fluorescent strain that was used to control for light scattering and cellular autofluorescence. *E. coli* strains MDG147 [MG1655 Φ(*ompF*$^+$-*yfp*$^+$) Φ(*ompC*$^+$-*cfp*$^+$)] [52] and EPB30 (MDG147 *envZ::kan*)[43] were employed for analysis of EnvZ signal output. Plasmid pRD400[40] retains the IPTG-based induction of EnvZ from plasmid pEnvZ[53] while adding a seven-residue linker (GGSSAAG)[54] and a C-terminal V5 epitope tag (GKPIPNPLLGLDST)[55]. As the C-terminus of bacterial receptors can be sensitive to the presence of an epitope tag, we previously ensured that the addition of a V5-epitope tag did not alter the signalling properties of EnvZ[40,56]. Plasmid pEB5[41] was employed as an empty control vector.

Selection of residues comprising TM2 of EnvZ

The primary sequence of EnvZ from *E. coli* K-12 MG1655 was subjected to DGpred using a minimal window of 9 residues and a maximal window of 40 residues[30]. Alternatively, a software

bioRxiv preprint doi: https://doi.org/10.1101/206888; this version posted October 27, 2017. The copyright holder for this preprint (which was not certified by peer review) is the author/funder. All rights reserved. No reuse allowed without permission.

305 package that identifies TM helices with a Markov model (TMHMM v2.0)[31] was also employed.
306 These software packages suggested that Leu-160 to Ile-181 and Leu-160 to Ile-179 comprise TM2
307 respectively. Based on these results and to maximize the probability of including all residues within
308 TM2, we targeted all residues between positions 156 to 184 for the creation of a library of single-
309 Cys-containing EnvZ receptors.
310
311 *Analysis of EnvZ signal output* in vivo
312
313 Bacterial cultures were grown as described previously[57] with minor modification. MDG147 or
314 EPB30 cells were transformed with pRD400 expressing one of the single-Cys-containing EnvZ
315 receptors or pEB5 (empty). Fresh colonies were used to inoculate 2-ml overnight cultures of
316 minimal medium A[58] supplemented with 0.2% glucose. Ampicillin, sucrose and IPTG were added
317 as appropriate. Cells were grown overnight at 37 °C and diluted at least 1:1000 into 7 ml of fresh
318 medium. Upon reaching an $OD_{600nm} \approx 0.3$, chloramphenicol was added to a final concentration of
319 170 μg/ml. Fluorescent analysis was immediately conducted with 2 ml of culture and a Varian Cary
320 Eclipse (Palo Alto, CA). CFP fluorescence was measured using an excitation wavelength of 434 nm
321 and an emission wavelength of 477 nm, while YFP fluorescence was measured using an excitation
322 wavelength of 505 nm and an emission wavelength of 527 nm. These values were corrected for cell
323 density and for light scattering/cellular autofluorescence by subtracting the CFP and YFP
324 fluorescence intensities determined for MG1655/pEB5 cells.
325
326 *Analysis of sulfhydryl-reactivity* in vivo
327
328 Cells were grown as described above with minor chnges. Upon reaching an $OD_{600nm} \sim 0.3$, cells
329 were subjected to between 250 μM molecular iodine for 10 min while incubating at 37 °C. The

bioRxiv preprint doi: https://doi.org/10.1101/206888; this version posted October 27, 2017. The copyright holder for this preprint (which was not certified by peer review) is the author/funder. All rights reserved. No reuse allowed without permission.

reaction was terminated with 8 mM N-ethylmaleimide (NEM) and 10 mM EDTA. Cells were harvested by centrifugation and resuspended in standard 6X non-reducing SDS-PAGE buffer supplemented with 12.5 mM NEM. Cell pellets were analysed on 10% SDS/acrylamide gels. Standard buffers and conditions were used for electrophoresis, immunoblotting and detection with enhanced chemiluminescence[59]. Anti-V5 (Invitrogen) was the primary antibody and peroxidase-conjugated anti-mouse IgG (Sigma) was the secondary antibody. Digitized images were acquired with a ChemiDoc MP workstation (Bio-RAD), analysed with ImageJ v1.49[60] and quantified with QtiPlot v0.9.8.10.

CG-MD simulations with SIDEKICK

As previously described[38], coarse-grained molecular dynamics (CG-MD) simulations were performed using the MARTINI forcefield with an approximately 4:1 mapping of non-H atoms to CG particles. Lennard-Jones interactions between 4 classes of particles: polar (P), charged (Q), mixed polar/apolar (N) and hydrophobic apolar (C) were used to treat interparticle interactions. Within MARTINI, P and C particle types were subdivided to reflect varying degrees of polarity. Short range electrostatic interactions were treated Coulombically, shifted to zero between 0 and 12 Å. Lennard-Jones interactions were shifted to zero between 9 and 12 Å. α-helix integrity was maintained via dihedral restraints. Peptide termini were treated as uncharged. Simulations were performed using Gromacs 3[61]. Temperature was coupled using a Berendsen thermostat at 323 K (τ_T=1 ps), and pressure was coupled semi-isotropically (across XY/Z) at 1 bar (compressibility=3×10^{-5} bar^{-1}, τ_P=10 ps). The initial simulation timestep was 20 fs. Initial models of the TM α-helices were generated as ideal, atomistically detailed α-helices using standard backbone angles and side- chain conformers. These were then converted to coarse-grained as

bioRxiv preprint doi: https://doi.org/10.1101/206888; this version posted October 27, 2017. The copyright holder for this preprint (which was not certified by peer review) is the author/funder. All rights reserved. No reuse allowed without permission.

described previously[38]. Around 128 DPPC molecules were used in each simulation along with around 3000 CG water particles, giving a final system size of ~65×65×13 Å.

Author contributions

R. Y., T. L. N, B. A. H. and R. R. D. conceived and designed the experiments. R. Y., T. L. N., A. H. and R. J. L. performed the experiments. R. Y., A. H., T. L. N., R. J. L., B. A. H. and R. R. D. analysed the data. R. Y., T. L. N., B. A. H. and R. R. D. wrote the manuscript. All authors read and approved the final manuscript.

Acknowledgments

R. Y. was generously supported by the Indonesia Endowment Fund for Education, Ministry of Finance (S-4833/LPDP.3/2015). T. L. N. was supported by a grant from the Erasmus+ programme. R. R. D. was supported with start-up funding from the Faculty of Science and from the Institute of Biological and Biomedical Science (IBBS) at the University of Portsmouth. B. A. H. was supported by The Royal Society (UF130039).

Competing interests

The authors declare no competing financial interests.

Figure legends

bioRxiv preprint doi: https://doi.org/10.1101/206888; this version posted October 27, 2017. The copyright holder for this preprint (which was not certified by peer review) is the author/funder. All rights reserved. No reuse allowed without permission.

Figure 1. EnvZ functions as a homodimer with a cytoplasmic N-terminus, the first transmembrane helix (TM1, white), a large periplasmic domain (sensor, white), the second transmembrane helix (TM2, red), a membrane-adjacent HAMP domain (grey) and the cytoplasmic domains responsible for dimerization and histidylphosphortransfer (DHp, black) and catalytic ATPase activity (CA, black). The position of the original Cys-277 residue that was mutated to Ala to produce the Cys-less EnvZ is provided. The residues subjected to Cys substitution and their position in the primary sequence is provided. Signal output from each single-Cys-containing variant is compared to the Cys-less (C277A) variant: less than 50% of Cys-less (light blue), between 50% and 75% of Cys-less (dark blue), between 75% and 125% of Cys-less (grey), between 125% and 200% (dark red) and greater than 200% (light red). Residue positions exhibited flipped signal output are indicated with a plus. The extent of sulphydryl-reactivity is also presented in five categories based on dimer-to-monomer ratio: no dimer present (white), less than 0.05 (light grey), between 0.05 and 0.2 (medium grey), between 0.2 and 0.5 (dark grey) and greater than 0.5 (red). Positions that exhibit a significant change in cross-linking between the low- and high-osmolarity regimes are indicated with a plus.

Figure 2. Signal output from the library of single-Cys EnvZ variants. (A) CFP/YFP from EPB30/pRD400 cells expressing one of single-Cys variants grown under the low-osmolarity (0% sucrose) regime. On the right axis, these CFP/YFP ratios are compared to the Cys-less (C277A) variant. (B) Magnified version of panel A in order to emphasise the region up to a 2-fold increase in CFP/YFP. (C) CFP/YFP from EPB30/pRD400 cells expressing one of the single-Cys variants grown under the high-osmolarity (15% sucrose) regime. On the right axis, these CFP/YFP ratios are compared to the Cys-less (C277A) variant. The flipped mutants are highlighted with a red dot in panel A (increased signal output) and a blue dot in panel C (decreased signal output). The shaded areas represent the mean signal output from the Cys-less variant of EnvZ with a range of one

bioRxiv preprint doi: https://doi.org/10.1101/206888; this version posted October 27, 2017. The copyright holder for this preprint (which was not certified by peer review) is the author/funder. All rights reserved. No reuse allowed without permission.

standard error of mean. These values are provided to aid in comparison. Error bars represent standard deviation of the mean with a sample size of $n \geq 3$.

Figure 3. Extent of sulfhydryl-reactivity for each single-Cys-containing EnvZ variant. EPB30/pRD400 cells were grown under the low- (empty circles, 0% sucrose) or high-osmolarity (filled circles, 15% sucrose) regimes and subjected to 250 μM molecular iodine for 10 minutes when their OD_{600nm} reached approximately 0.25. As shown in Figure S5, this allowed us to determine the dimer/monomer ratio represented on the Y-axis. Three distinct regions, denoted I, II and III were observed and are described in the text. Error bars represent the standard error of the mean with a sample size of $n \geq 3$.

Figure 4. Aromatic tuning and signal output from EnvZ. (A) When aromatic tuning was performed in EnvZ, a Trp-Leu-Phe triplet (red) was repositioned within the C-terminal region of TM2. (B) Helix displacements, (C) tilt distributions and (D) azimuthal rotational distributions of the aromatically tuned EnvZ TM2 helices. Histograms are shown for all time points of all membranes of each ensemble. Aromatically tuned mutants have been classified based on their signal output into five categories: highly kinase biased (WLF-1; pink), moderately kinase biased (WLF-5, WLF-4, WLF-3; red), balanced (wild-type; black), moderately phosphatase biased (WLF-2, WLF+1, dark blue) and highly phosphatase biased (WLF+2, light blue).

References

1 *Delcour, A. H. Solute uptake through general porins. Frontiers in bioscience : a journal and virtual library **8**, d1055-1071, (2003).*

2 *Nikaido, H. Molecular basis of bacterial outer membrane permeability revisited. Microbiology and molecular biology reviews : MMBR **67**, 593-656, (2003).*

3 *Elliott, E. et al. In vivo development of ertapenem resistance in a patient with pneumonia caused by Klebsiella pneumoniae with an extended-spectrum beta-lactamase. Clinical*

bioRxiv preprint doi: https://doi.org/10.1101/206888; this version posted October 27, 2017. The copyright holder for this preprint (which was not certified by peer review) is the author/funder. All rights reserved. No reuse allowed without permission.

infectious diseases : an official publication of the Infectious Diseases Society of America ***42****, e95-98, (2006).*

4 *Hernandez-Alles, S. et al. Relationship between outer membrane alterations and susceptibility to antimicrobial agents in isogenic strains of Klebsiella pneumoniae. The Journal of antimicrobial chemotherapy* ***46****, 273-277, (2000).*

5 *Jacoby, G. A., Mills, D. M. & Chow, N. Role of beta-lactamases and porins in resistance to ertapenem and other beta-lactams in Klebsiella pneumoniae. Antimicrob. Agents Chemother.* ***48****, 3203-3206, (2004).*

6 *Kaczmarek, F. M., Dib-Hajj, F., Shang, W. & Gootz, T. D. High-level carbapenem resistance in a Klebsiella pneumoniae clinical isolate is due to the combination of bla(ACT-1) beta-lactamase production, porin OmpK35/36 insertional inactivation, and down-regulation of the phosphate transport porin phoe. Antimicrob. Agents Chemother.* ***50****, 3396-3406, (2006).*

7 *Loli, A. et al. Sources of diversity of carbapenem resistance levels in Klebsiella pneumoniae carrying blaVIM-1. The Journal of antimicrobial chemotherapy* ***58****, 669-672, (2006).*

8 *Martinez-Martinez, L. et al. Activities of imipenem and cephalosporins against clonally related strains of Escherichia coli hyperproducing chromosomal beta-lactamase and showing altered porin profiles. Antimicrob. Agents Chemother.* ***44****, 2534-2536, (2000).*

9 *Mena, A. et al. Characterization of a large outbreak by CTX-M-1-producing Klebsiella pneumoniae and mechanisms leading to in vivo carbapenem resistance development. J Clin Microbiol* ***44****, 2831-2837, (2006).*

10 *Egger, L. A. & Inouye, M. Purification and characterization of the periplasmic domain of EnvZ osmosensor in Escherichia coli. Biochem. Biophys. Res. Commun.* ***231****, 68-72, (1997).*

11 *Forst, S. A. & Roberts, D. L. Signal transduction by the EnvZ-OmpR phosphotransfer system in bacteria. Research in microbiology* ***145****, 363-373, (1994).*

12 *Mizuno, T. His-Asp phosphotransfer signal transduction. J Biochem* ***123****, 555-563, (1998).*

13 *Hoch, J. A. & Silhavy, T. J. (American Society of Microbiology Press, Washington, DC, USA, 1995).*

14 *Gerken, H., Charlson, E. S., Cicirelli, E. M., Kenney, L. J. & Misra, R. MzrA: a novel modulator of the EnvZ/OmpR two-component regulon. Mol Microbiol* ***72****, 1408-1422, (2009).*

15 *Gerken, H. & Misra, R. MzrA-EnvZ interactions in the periplasm influence the EnvZ/OmpR two-component regulon. J Bacteriol* ***192****, 6271-6278, (2010).*

16 *Forst, S. A., Delgado, J. & Inouye, M. DNA-binding properties of the transcription activator (OmpR) for the upstream sequences of ompF in Escherichia coli are altered by envZ mutations and medium osmolarity. J Bacteriol* ***171****, 2949-2955, (1989).*

17 *Lan, C. Y. & Igo, M. M. Differential expression of the OmpF and OmpC porin proteins in Escherichia coli K-12 depends upon the level of active OmpR. J Bacteriol* ***180****, 171-174, (1998).*

18 *Russo, F. D. & Silhavy, T. J. EnvZ controls the concentration of phosphorylated OmpR to mediate osmoregulation of the porin genes. J Mol Biol* ***222****, 567-580, (1991).*

19 *Adler, M., Anjum, M., Andersson, D. I. & Sandegren, L. Combinations of mutations in envZ, ftsI, mrdA, acrB and acrR can cause high-level carbapenem resistance in Escherichia coli. The Journal of antimicrobial chemotherapy* ***71****, 1188-1198, (2016).*

20 *Gushchin, I. et al. Mechanism of transmembrane signaling by sensor histidine kinases. Science, (2017).*

21 *Unnerstale, S., Maler, L. & Draheim, R. R. Structural characterization of AS1-membrane interactions from a subset of HAMP domains. Biochim Biophys Acta* ***1808****, 2403-2412, (2011).*

bioRxiv preprint doi: https://doi.org/10.1101/206888; this version posted October 27, 2017. The copyright holder for this preprint (which was not certified by peer review) is the author/funder. All rights reserved. No reuse allowed without permission.

22 *Hulko, M. et al. The HAMP domain structure implies helix rotation in transmembrane signaling. Cell **126**, 929-940, (2006).*

23 *Zhou, Q., Ames, P. & Parkinson, J. S. Mutational analyses of HAMP helices suggest a dynamic bundle model of input-output signalling in chemoreceptors. Mol Microbiol **73**, 801-814, (2009).*

24 *Falke, J. J. & Hazelbauer, G. L. Transmembrane signaling in bacterial chemoreceptors. Trends in biochemical sciences **26**, 257-265, (2001).*

25 *Hazelbauer, G. L., Falke, J. J. & Parkinson, J. S. Bacterial chemoreceptors: high-performance signaling in networked arrays. Trends in biochemical sciences **33**, 9-19, (2008).*

26 *Parkinson, J. S., Hazelbauer, G. L. & Falke, J. J. Signaling and sensory adaptation in Escherichia coli chemoreceptors: 2015 update. Trends in microbiology **23**, 257-266, (2015).*

27 *Hwang, E. et al. Crystal structure of the EnvZ periplasmic domain with CHAPS. FEBS Lett **591**, 1419-1428, (2017).*

28 *Upadhyay, A. A., Fleetwood, A. D., Adebali, O., Finn, R. D. & Zhulin, I. B. Cache Domains That are Homologous to, but Different from PAS Domains Comprise the Largest Superfamily of Extracellular Sensors in Prokaryotes. PLoS computational biology **12**, e1004862, (2016).*

29 *Heininger, A., Yusuf, R., Lawrence, R. & Draheim, R. R. Identification of transmembrane helix 1 (TM1) surfaces important for EnvZ dimerisation and signal output. Biochim. Biophys. Acta **1858**, 1868-1875, (2016).*

30 *Hessa, T. et al. Molecular code for transmembrane-helix recognition by the Sec61 translocon. Nature **450**, 1026-1030, (2007).*

31 *Krogh, A., Larsson, B., von Heijne, G. & Sonnhammer, E. L. Predicting transmembrane protein topology with a hidden Markov model: application to complete genomes. J Mol Biol **305**, 567-580, (2001).*

32 *Adase, C. A., Draheim, R. R. & Manson, M. D. The residue composition of the aromatic anchor of the second transmembrane helix determines the signaling properties of the aspartate/maltose chemoreceptor Tar of Escherichia coli. Biochemistry **51**, 1925-1932, (2012).*

33 *Adase, C. A., Draheim, R. R., Rueda, G., Desai, R. & Manson, M. D. Residues at the cytoplasmic end of transmembrane helix 2 determine the signal output of the TarEc chemoreceptor. Biochemistry **52**, 2729-2738, (2013).*

34 *Wright, G. A., Crowder, R. L., Draheim, R. R. & Manson, M. D. Mutational analysis of the transmembrane helix 2-HAMP domain connection in the Escherichia coli aspartate chemoreceptor tar. J Bacteriol **193**, 82-90, (2011).*

35 *Bass, R. B., Butler, S. L., Chervitz, S. A., Gloor, S. L. & Falke, J. J. Use of site-directed cysteine and disulfide chemistry to probe protein structure and dynamics: applications to soluble and transmembrane receptors of bacterial chemotaxis. Methods in enzymology **423**, 25-51, (2007).*

36 *Draheim, R. R., Bormans, A. F., Lai, R. Z. & Manson, M. D. Tuning a bacterial chemoreceptor with protein-membrane interactions. Biochemistry **45**, 14655-14664, (2006).*

37 *Botelho, S. C., Enquist, K., von Heijne, G. & Draheim, R. R. Differential repositioning of the second transmembrane helices from E. coli Tar and EnvZ upon moving the flanking aromatic residues. Biochim Biophys Acta **1848**, 615-621, (2015).*

38 *Hall, B. A., Armitage, J. P. & Sansom, M. S. Transmembrane helix dynamics of bacterial chemoreceptors supports a piston model of signalling. PLoS computational biology **7**, e1002204, (2011).*

39 *Mise, T. Structural Analysis of the Ligand-Binding Domain of the Aspartate Receptor Tar from Escherichia coli. Biochemistry **55**, 3708-3713, (2016).*

bioRxiv preprint doi: https://doi.org/10.1101/206888; this version posted October 27, 2017. The copyright holder for this preprint (which was not certified by peer review) is the author/funder. All rights reserved. No reuse allowed without permission.

40 *Norholm, M. H., von Heijne, G. & Draheim, R. R. Forcing the Issue: Aromatic Tuning Facilitates Stimulus-Independent Modulation of a Two-Component Signaling Circuit. ACS Synth Biol **4**, 474-481, (2015).*

41 *Batchelor, E. & Goulian, M. Robustness and the cycle of phosphorylation and dephosphorylation in a two-component regulatory system. Proc Natl Acad Sci U S A **100**, 691-696, (2003).*

42 *Miyashiro, T. & Goulian, M. High stimulus unmasks positive feedback in an autoregulated bacterial signaling circuit. Proc Natl Acad Sci U S A **105**, 17457-17462, (2008).*

43 *Siryaporn, A. & Goulian, M. Cross-talk suppression between the CpxA-CpxR and EnvZ-OmpR two-component systems in E. coli. Mol Microbiol **70**, 494-506, (2008).*

44 *Chervitz, S. A. & Falke, J. J. Molecular mechanism of transmembrane signaling by the aspartate receptor: a model. Proc Natl Acad Sci U S A **93**, 2545-2550, (1996).*

45 *Falke, J. J. Piston versus Scissors: Chemotaxis Receptors versus Sensor His-Kinase Receptors in Two-Component Signaling Pathways. Structure **22**, 1219-1220, (2014).*

46 *Molnar, K. S. et al. Cys-Scanning Disulfide Crosslinking and Bayesian Modeling Probe the Transmembrane Signaling Mechanism of the Histidine Kinase, PhoQ. Structure **22**, 1239-1251, (2014).*

47 *Cheung, J., Bingman, C. A., Reyngold, M., Hendrickson, W. A. & Waldburger, C. D. Crystal structure of a functional dimer of the PhoQ sensor domain. J Biol Chem **283**, 13762-13770, (2008).*

48 *Inouye, M. Signaling by transmembrane proteins shifts gears. Cell **126**, 829-831, (2006).*

49 *Yusuf, R. & Draheim, R. R. Employing aromatic tuning to modulate output from two-component signaling circuits. J Biol Eng **9**, 7, (2015).*

50 *Casadaban, M. J. & Cohen, S. N. Analysis of gene control signals by DNA fusion and cloning in Escherichia coli. J Mol Biol **138**, 179-207, (1980).*

51 *Guyer, M. S., Reed, R. R., Steitz, J. A. & Low, K. B. Identification of a sex-factor-affinity site in E. coli as gamma delta. Cold Spring Harb Symp Quant Biol **45 Pt 1**, 135-140, (1981).*

52 *Batchelor, E., Silhavy, T. J. & Goulian, M. Continuous control in bacterial regulatory circuits. J Bacteriol **186**, 7618-7625, (2004).*

53 *Hsing, W. & Silhavy, T. J. Function of conserved histidine-243 in phosphatase activity of EnvZ, the sensor for porin osmoregulation in Escherichia coli. J Bacteriol **179**, 3729-3735, (1997).*

54 *Cantwell, B. J. et al. CheZ phosphatase localizes to chemoreceptor patches via CheA-short. J Bacteriol **185**, 2354-2361, (2003).*

55 *Southern, J. A., Young, D. F., Heaney, F., Baumgartner, W. K. & Randall, R. E. Identification of an epitope on the P and V proteins of simian virus 5 that distinguishes between two isolates with different biological characteristics. The Journal of general virology **72 (Pt 7)**, 1551-1557, (1991).*

56 *Lai, R. Z., Bormans, A. F., Draheim, R. R., Wright, G. A. & Manson, M. D. The region preceding the C-terminal NWETF pentapeptide modulates baseline activity and aspartate inhibition of Escherichia coli Tar. Biochemistry **47**, 13287-13295, (2008).*

57 *Lehning, C. E., Heidelberger, J. B., Reinhard, J., Norholm, M. H. & Draheim, R. R. A Modular High-Throughput In Vivo Screening Platform Based on Chimeric Bacterial Receptors. ACS Synth Biol, (2017).*

58 *Miller, J. H. A Short Course in Bacterial Genetics: A Laboratory Manual and Handbook for Escherichia coli and Related Bacteria. (Cold Spring Harbor Laboratory Press, 1992).*

59 *Ausubel, F. M. et al. Current Protocols in Molecular Biology. (Wiley, 1998).*

60 *Schneider, C. A., Rasband, W. S. & Eliceiri, K. W. NIH Image to ImageJ: 25 years of image analysis. Nat Methods **9**, 671-675, (2012).*

bioRxiv preprint doi: https://doi.org/10.1101/206888; this version posted October 27, 2017. The copyright holder for this preprint (which was not certified by peer review) is the author/funder. All rights reserved. No reuse allowed without permission.

61 *Van Der Spoel, D. et al. GROMACS: fast, flexible, and free. Journal of computational chemistry **26**, 1701-1718, (2005).*

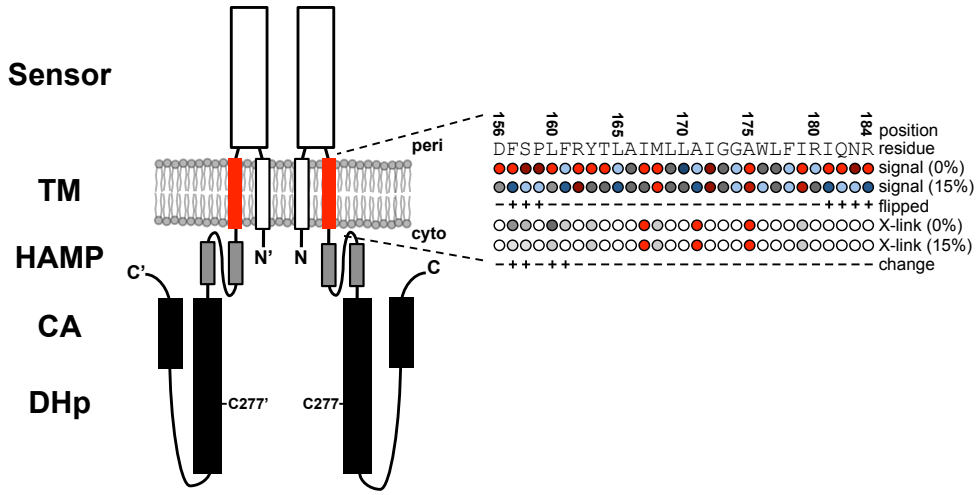
Sensor
TM
HAMP
CA
DHp
peri
cyto
N'
N
C'
C
C277'
C277
156
160
165
170
175
180
184
position
DFSPLFRYTLAIMLLAIGGAWLFIRIQNR
residue
signal (0%)
signal (15%)
flipped
X-link (0%)
X-link (15%)
change

Figure 1.

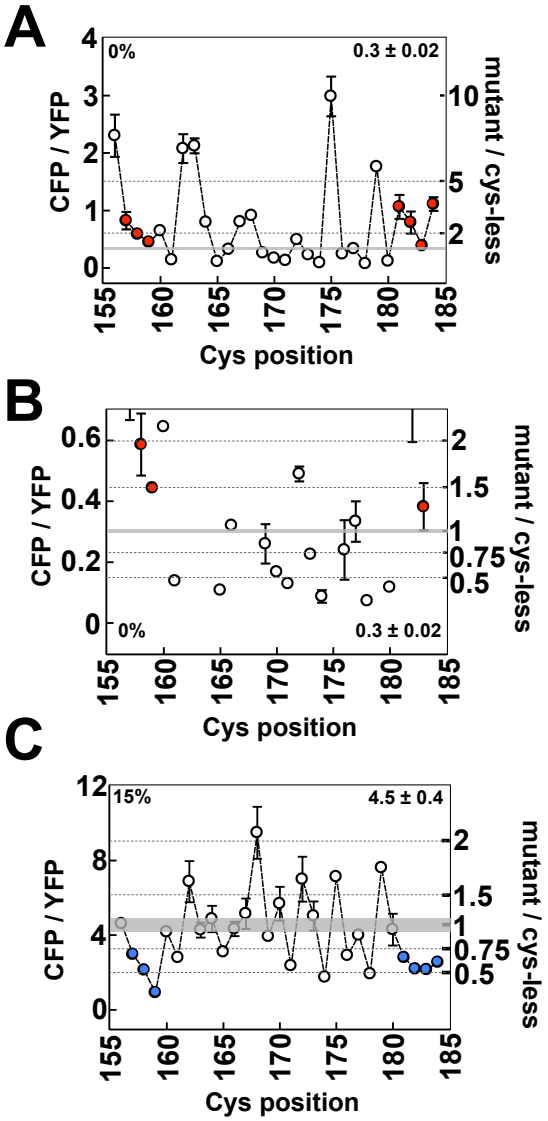
A
0%
0.3 ± 0.02
CFP / YFP
mutant / cys-less
Cys position
B
0%
0.3 ± 0.02
CFP / YFP
mutant / cys-less
Cys position
C
15%
4.5 ± 0.4
CFP / YFP
mutant / cys-less
Cys position

Figure 2.

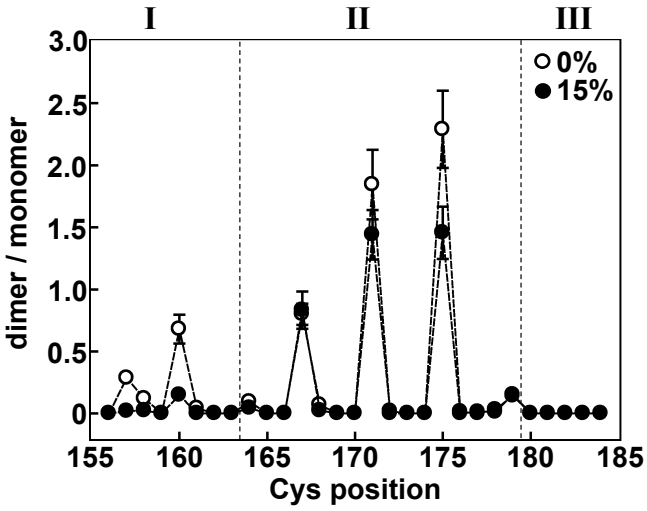
I
II
III
0%
15%
dimer / monomer
3.0
2.5
2.0
1.5
1.0
0.5
0
155
160
165
170
175
180
185
Cys position

Figure 3.

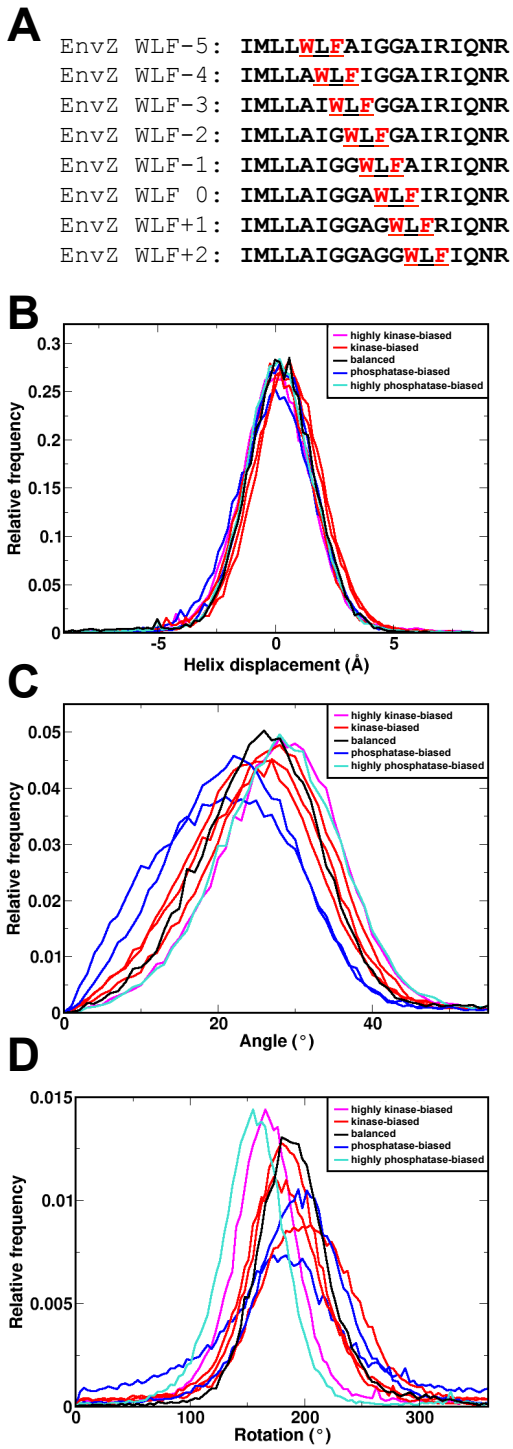
A
EnvZ WLF-5: IMLLWLFAIGGAIRIQNR
EnvZ WLF-4: IMLLAWLFIGGAIRIQNR
EnvZ WLF-3: IMLLAIWLFGGAIRIQNR
EnvZ WLF-2: IMLLAIGWLFGAIRIQNR
EnvZ WLF-1: IMLLAIGGWLFAIRIQNR
EnvZ WLF 0: IMLLAIGGAWLFIRIQNR
EnvZ WLF+1: IMLLAIGGAGWLFRIQNR
EnvZ WLF+2: IMLLAIGGAGGWLFIQNR
B
highly kinase-biased
kinase-biased
balanced
phosphatase-biased
highly phosphatase-biased
Relative frequency
Helix displacement (Å)
C
Angle (°)
D
Rotation (°)

Figure 4.